Solid Freeform Fabrication 2023: Proceedings of the 34th Annual International Solid Freeform Fabrication Symposium – An Additive Manufacturing Conference
Reviewed Paper

THERMAL SIMULATION OF THE MATERIAL EXTRUSION PROCESS WITH DIFFERENT PRINT BED BOUNDARY CONDITIONS

Orkhan Huseynov*, Mohammad Al-Shaikh Ali* and Ismail Fidan†

*Department of Mechanical Engineering
†Department of Manufacturing and Engineering Technology
College of Engineering
Tennessee Technological University
Cookeville, TN 38505

Abstract

The temperature evolution in the material extrusion (MEX) process significantly affects the stability and bonding of 3D printed parts. Numerous studies have focused on developing models to capture the temperature history of the MEX process. However, there remains a need to explore the influence of different boundary conditions applied to the print bed. Additionally, the size of the bed relative to the 3D printed object has not been extensively investigated. This study aims to analyze the thermal behavior of the first layer in MEX by considering various boundary conditions and bed sizes. The obtained results will contribute to the development of faster yet reliable models for simulating the temperature variation in the MEX process.

Keywords: Additive Manufacturing, Material Extrusion, Thermal simulation, Print bed, Thermal history

Introduction

Material Extrusion (MEX) manufacturing is a heat-driven process where the bonding of the additively formed layers is achieved by the thermal energy supplied inside the extruder. However, the rapidly changing thermal gradients during the process can affect the microstructure of the 3d printed parts thereby, the macrostructure of the ready product [1–5]. Therefore, it is crucial to have information about the thermal evolution as a function of time to predict the bonding quality and mechanical properties of the final printed product as well as the strength of the parts [6–8]. Understanding the thermal history is essential for preventing formation of defects, improving surface quality, and enhancing mechanical properties. According to Das et al., in the years between 2015 and 2020, 28 different models have been developed for the thermal evolution of the Material Extrusion (MEX) process [9]. These models investigated various process and 3D printing parameters. Costa et al. studied the influence of the different heat transfer mechanisms between filaments, filament and environment, filament and bed. The researchers found that convection with ambient air, heat transfer between neighboring filaments and print bed (also called, build plate) have the highest impact [10]. Cattenone et al. investigated the different element and time step sizes for the thermal simulation. According to the analysis results, time step size influences the local temperature distribution, particularly, observed activation temperature. Furthermore, for descent models, larger element sizes compared to filament dimensions can be used without significant loss of accuracy [11].

Prajapati et al. conducted experiments to measure the temperature drop in standoff region between nozzle tip and print bed. Their findings indicated that the temperature in this region does not change significantly in the region, except under extreme cases [12]. Trofimov et al. studied the distortion created by the temperature history of a printed PLA bridge structure. The research team also showed the extensive Infrared (IR) camera imaging of the temperature variations in the cubic sample for validation [13]. Compton et al. used a 1D heat transfer model to predict the temperature variation for the thin wall structure model made of short carbon fiber 20% wt. ABS material. They calculated the Biot number to decrease dimensionality of the problem and as a result, approximated each layer as an isothermal solid volume. The authors used a 1-D finite difference method to evaluate the temperature evolution of the printed part and then compared the results with the thermal camera. The team concluded that for the successful print of the large objects the chamber temperature has the most significant effect, therefore its value must be increased. They also found that a higher thermal conductivity has a negative influence on the geometric stability of the printed parts [14].

Friedrich II et al. investigated the temperature evolution of pyramid structure printed from Acrylonitrile Butadiene Styrene (ABS) material and compared the simulation results with Infrared (IR) camera observations. The model and experiment agree with 5 % error. According to the research results, exponential heat loss occurs and that as the layer print time decreases, the average temperature increases [15, 16]. Another study focused on the two main aspects of the MEX: determining the correct value of the heat transfer coefficient and studying the influence of the numerical simulations on gyroid and rectilinear infill structures using Polylactic Acid (PLA) material. By varying the ambient temperature around the build and the heat transfer coefficient, the researchers found the correct value that matched simulation and experimental results. They also discovered that excluding the air voids in the simulation did not significantly significant influence the nodal temperature results [17]. Multi-scale modeling approaches have also been used to predict the material properties of composite parts manufactured by MEX [18].

Despite the mentioned simulations conducted for MEX, there is no consensus on the applied boundary conditions for the bed. Different approaches have been followed in this case such as inclusion of the great portion of the print bed with different material properties with perfect contact [13], assuming contact resistance between first elements and bed [10], applying the bed temperature directly to the attached nodes [11] etc. Thus, the aim of the paper is to investigate the comparative influence of the boundary conditions in bed using different parameters such as changing bed size and to examine the effects of the similar boundary conditions on the bed. The results of this paper will provide insights into the thermal processes occurring in the first layer and highlight the challenges in the simulation process.

Material and methods

PLA is used for the study with material properties given in [19]. Process parameters are given in Table 1. The nozzle activation temperature was selected to be 150°C due to the availability of the experimental values published in [13].

Table 1 Basic parameters used for validation study

Nozzle diameter and velocity	0.4 mm and 30 mm/sec
Extrusion temperature	150 °C
Bed temperature	52 °C
Infill density	100 %
Convective heat transfer coefficient for the printed part	$71\ \frac{W}{m^2 °C}$
Convective heat transfer coefficient for the bed	$5\ \frac{W}{m^2 °C}$
Ambient temperature	60°C
Number of layers	1

Selected body for simulation is as shown in Figure 1. The dimensions of the 3D printed object have 1 layer height in y direction (0.2 mm) and 60 mm in x direction and 10 mm in z direction. MEX process happens in xz plane and nozzle moves in x direction with a zigzag pattern provided by the g-code. Part is sliced with PrusaSlicer.

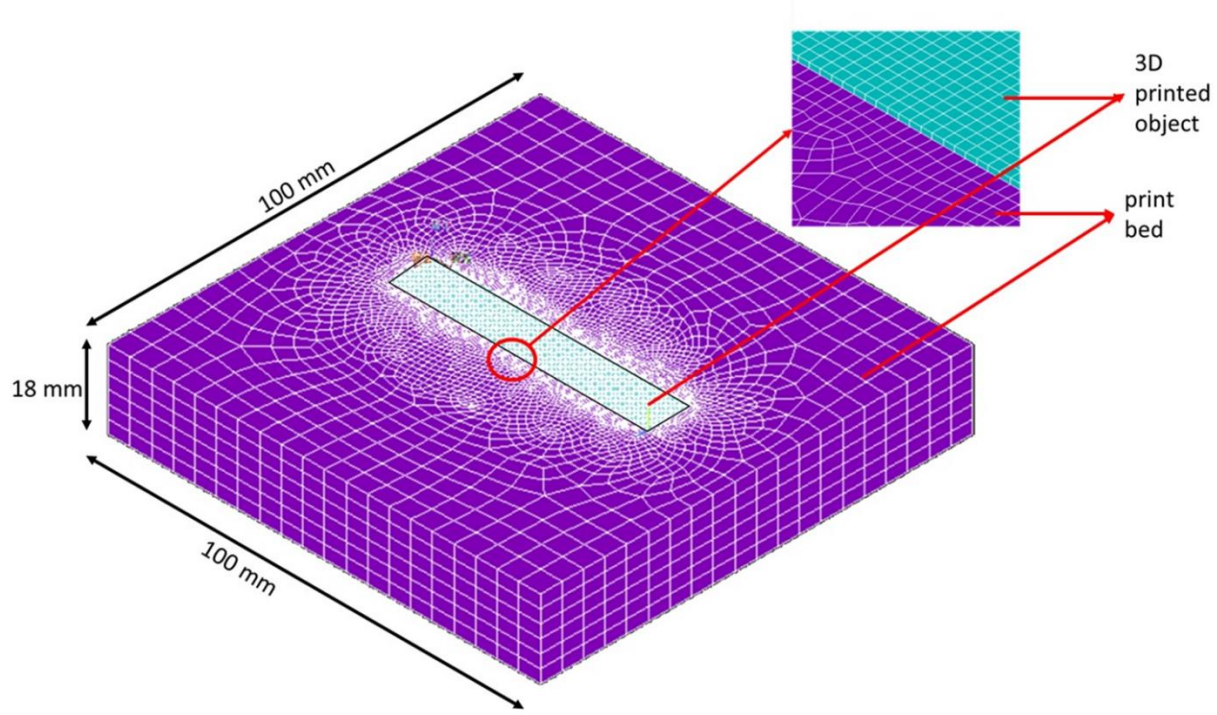

Figure 1. Geometric description of the simulated bodies

For the simulation strategy, parameter variation is selected as shown in Table 2. In the first 4 cases (S1, S2, S3 and S4), print bed dimensions have been varied. For those mentioned simulations, bottom nodes that are attached to the bed as also shown in Figure 2 are allowed to have conduction with the bed and hence, they share the nodes. In the meantime, the exteriors of the bed have convective heat transfer and the bottom part of the bed is at specified bed temperature. While in case S5, S6 and S7, the bed is not simulated but the conditions of the bed are imposed on

the attached nodes. Particularly, in case S5, the attached nodes are at 52°C, in S6 and S7, those nodes have contact resistance with 2 extreme values.

Table 2. Design of Parameters for the simulation

Simulation strategy	**Bed size**	**Boundary condition on attached nodes**
S1	100 mm x 100 mm x 18 mm	i) $T_{bottom\ of\ the\ bed\ bed} = T_{bed}$ ii) convection from bed exterior iii) conduction with bed and deposited filament nodes $\frac{k_{bed}\partial T}{\partial \hat{n}} + \dot{q}_{cv}^{bed\ ext} = 0$, [13]
S2	100 mm x 100 mm x 3 mm	
S3	60 mm x 60 mm x 3 mm	
S4	60 mm x 10 mm x 0.2 mm	
S5	-	Attached filament nodes are at bed temperature, $T_{\Omega}(t) = T_b$ on $\Omega(t)$, [11]
S6	-	Contact conductance with the print bed, $h_{contact} = 30\frac{W}{m^2K}$ [10], $\frac{k_{filament}\partial T}{\partial \hat{n}} + \dot{q}_{cv}^{bed-filament} + \dot{q}_{cv}^{filament-ambient} = 0$
S7	-	Contact conductance with the print bed, $h_{contact} = 1500\frac{W}{m^2K}$, $\frac{k_{filament}\partial T}{\partial \hat{n}} + \dot{q}_{cv}^{bed-filament} + \dot{q}_{cv}^{filament-ambient} = 0$

The MEX process is simulated using the "birth and death function" of Ansys Parametric Design Language (APDL) where each deposited element is progressively activated. The simulation strategy for temperature in 3D printing is a transient thermal analysis hence performed using a moving local coordinate system and applies to real-time deposition process. The simulation begins with the activation of the first element at the nozzle temperature. The boundary conditions are then applied to the element, and the simulation is run for a given time step size. After the time step has elapsed, the next neighboring element is activated. Before activation, the boundary conditions in the nodes that are shared between the activated element and to be activated one are removed. The newly activated element then has the respective boundary conditions applied to it. This process is repeated until all the elements in the model have been activated. Essentially, the simulation strategy combines moving heat source and material addition (deposition) process. The use of a moving local coordinate system in the simulation allows for the accurate modeling of the heat transfer that occurs during the 3D printing process. The moving coordinate system follows the nozzle as it travels across the build platform, which ensures that the boundary conditions are applied correctly to each element in the model. Temperature field for transient thermal problem can be stated as follows:

$$\frac{\rho c_p \partial T}{\partial t} = \nabla(k\nabla T) + \dot{q}_{generation} \quad (1)$$

where T is the temperature, t is the time, c_p specific heat value in $\frac{J}{kgK}$, ρ density in $\frac{kg}{m^3}$, k is the thermal conductivity (generally for printed materials it is not isotropic), $\dot{q}_{generation}$ represents the rate of external volumetric heat source in $\frac{J}{m^3}$. Boundary condition of the body is function of time and external surfaces are always in convection and radiation heat transport with the surroundings. The temperature of the environment is assumed to be constant and not affected by the bed temperature.

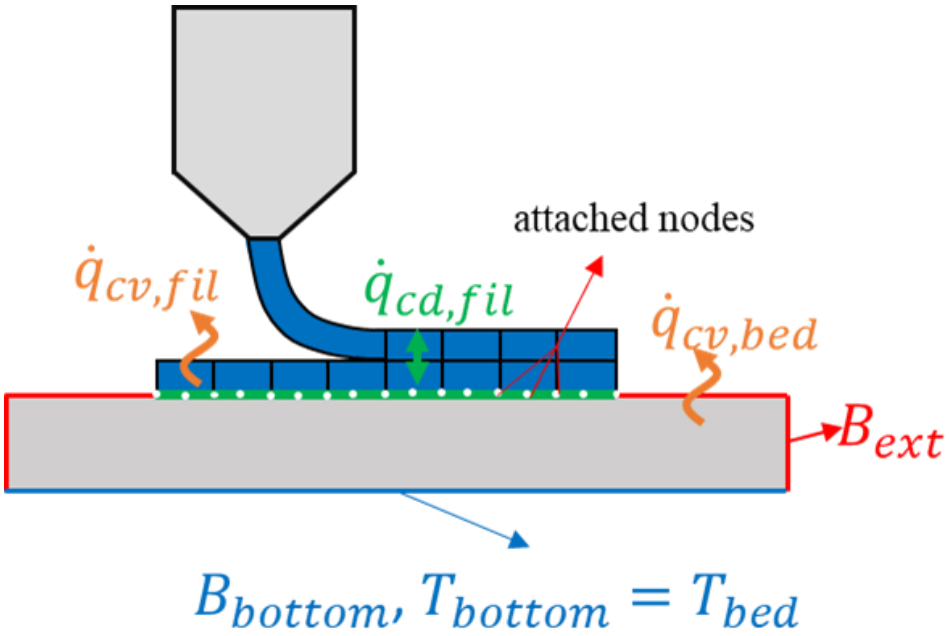

Figure 2. Boundary conditions for the simulated part

The first layer elements are in contact with the build plate and assumed to have different boundary conditions as specified above. Knowing the temperature of bed as T_b, then

$$T_\Omega(t) = T_b \text{ on } \Omega(t) \quad (2)$$

Then there may be different boundary equations as stated in Table 2. For S1 to S4, the governing boundary terms are

$$\frac{k_{bed}\partial T}{\partial \hat{n}} + \dot{q}_{cv}^{bed\ ext} = 0 \quad (3)$$

where $\dot{q}_{cv}^{bed\ ext}$ is the convective heat transfer between bed and ambient air, $h_{bed}(T - T_{bed})$.

If the attached nodes to the bed are assumed to be at bed temperature, then equation 2 can be used.

For cases S6 and S7, using thermal contact conductance h_{bed} with units of $\frac{W}{m^{2\circ}C}$, the heat transfer boundary condition between the bed and filament can be written as

$$\frac{k_{filament}\partial T}{\partial \hat{n}} + \dot{q}_{cv}^{bed-filament} = 0 \quad (4)$$

where

$$\dot{q}_{cv}^{bed-filament} = h_{bed}(T - T_{bed}) \quad (5)$$

For contact elements, TARGE170 was used for the print bed and CONTA174 used for the 3D printed part. The boundary condition for the other elements is the balance between convection heat transfer with environment and conduction heat transfer between the filaments, so

$$\frac{k_{filament}\partial T}{\partial \hat{n}} + \dot{q}_{cv}^{amb} = 0 \text{ and } \dot{q}_{cv}^{amb} = h_{amb}(T - T_{\infty}) \quad (6)$$

To determine the convective heat transfer coefficient for the filaments, Hilpert's data can be used for cylindrical shapes and given in Table 3 [20]

$$h_{cv} = \frac{Nu_D k_{air}}{D_{filament}} \quad (7)$$

where k_{air} is the thermal conductivity of air, Nu_D is the Nusselt number based of diameter which is found by correlation formulas in Table 3. Then

$$Nu_D = CRe^m Pr^{\frac{1}{3}} \quad (8)$$

Table 3 Empirical correlations for convective flow over cylinder [20]

Range of Reynolds number	**C (-)**	**M (-)**
0.4-4	0.989	0.330
4-40	0.911	0.385
40-4000	0.683	0.466
4000-40000	0.193	0.618
40000-400000	0.027	0.805

Results and discussion

In order to analyze the simulation results, two specific points were chosen, located at coordinates x=0.4 mm, z=0.4 mm, y=0 mm (on the print bed) and x=0.4 mm, z=0.4 mm, y=0.2 mm (top surface of the first element) and shown in Figure 3. The observed peaks in the temperature graphs are characteristic of the MEX process, resulting from the addition of new neighboring elements. In scenarios S6 and S7, the activated temperature of 150°C is applied to the attached nodes, and they are exposed to thermal resistance by bonded contact. The contact conductance value used in S6 is reported in [10].

As given in Figure 3, for simulation strategies of S1 to S4, the observed variations in peak temperatures are approximately 4°C. These scenarios represent different bed sizes, with S1 corresponding to the thickest bed size with largest dimensions, which provides the most extreme influence on the temperature profile representation. As the bed size decreases in S2, S3, and S4, the accuracy of the temperature predictions is reduced due to the smaller thermal mass and faster cooldown rates of the bed. Particularly, the first peak observed in S4 is larger than the others due to the reduced bed thickness and direct contact with the element. However, the second peak in S4 is the smallest among all scenarios (S1 to S4) and the primary reason for this is that during the second peak, heat transfer is conducted to the first element. Furthermore, since the cooling rate of

the newly activated element is very fast, the amount of time available for thermal energy transfer from this new element to the current one is minimal, resulting in a sharp but small temperature peak.

The heating of the bed in conduction case (S_1 to S_4) is different than the contact resistance cases of S_6 to S_7. In the conduction case, the nodes are shared between the bed and the element. When the new element is activated, the bottom nodes of that element are at bed temperature. Then those nodes are heated due to the conduction of the heat inside the element towards to those shared nodes. In comparison, when considering thermal resistance, the heat transfer is primarily driven by the newly introduced element, which heats the print bed that has different material and element identity in APDL, thus maintaining distinct thermal identities for the element and the bed. The resemblance can be explained as in the equation below.

$$\dot{Q}_{cd} = kA\frac{\Delta T}{\Delta x} = \left(\frac{k}{\Delta x}\right) A\,\Delta T = h_{cd}\,A\,\Delta T \qquad (9)$$

Using the element height of 0.2 mm and considering that the first node (distinct from the bed's temperature) is positioned at the center of the element (0.1 mm), the thermal transmittance or conductance value of h_{cd} within the component is calculated as approximately $\frac{0.15}{0.1\times10^{-3}} \sim 1500\,\frac{W}{m^2K}$ where $0.15\,\frac{W}{mK}$ is the typical polymer thermal conductivity. This value has the same order of magnitude to the thermal conductance used for bonded contact in S_7. Consequently, the self-heating of the shared node by the element itself exhibits a comparable order of magnitude to when the component heats the bed with a contact resistance of $1500\,\frac{W}{m^2K}$. It's worth noting that variations in the thermal conductivity of the printed body would yield different values for the contact resistance and thermal conduction, thereby influencing the overall heat transfer characteristics as in S_6.

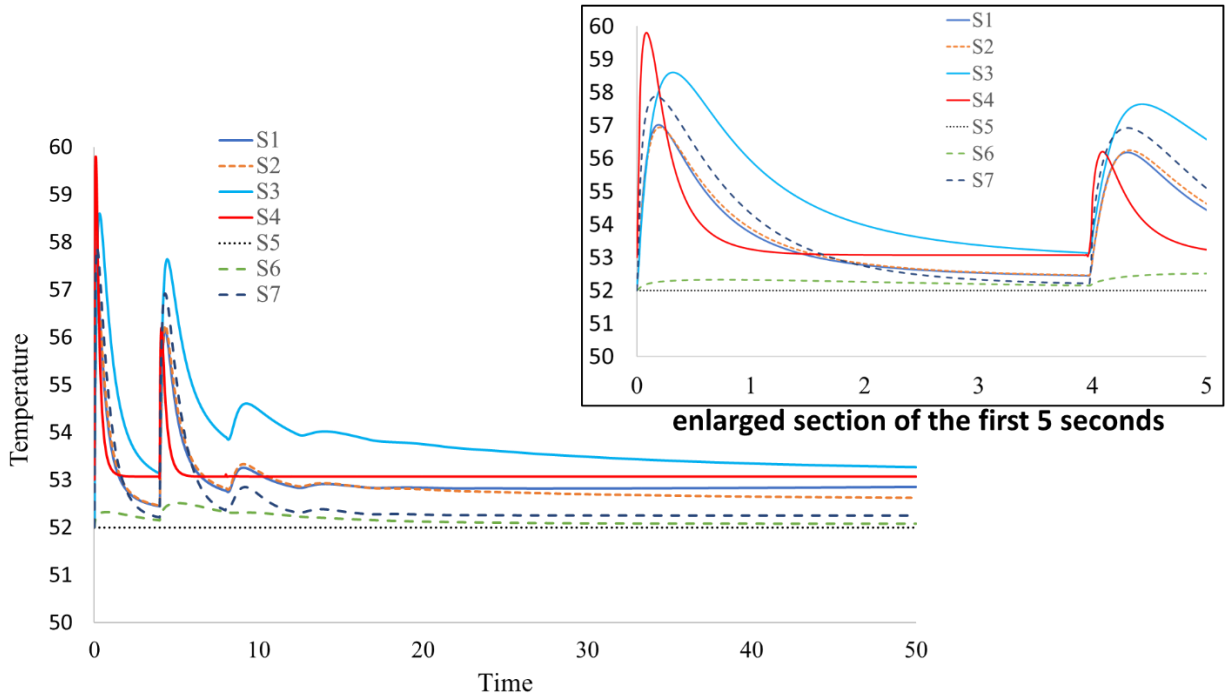

Figure 3. Variation of the temperature for the node at x=0.4 mm, z=0.4 mm, y=0 (on the bed)

The influence of higher thermal inertia is also evident in the contour plots shown in Figure 4 for two extreme cases of bed dimensions. In the case of the full bed size in S1, the temperature profile due to the birth of a new element significantly affects even the regions outside the 3D printed object. Conversely, in the case of a smaller bed size, the activation of the elements does not impact other regions, and the bed cools down rapidly through convective heat transfer. Additionally, the maximum nodal temperature values shown in Figure 4 differ between the two cases. For S1, the maximum nodal temperature is 56.68°C compared to 58.76°C in S4.

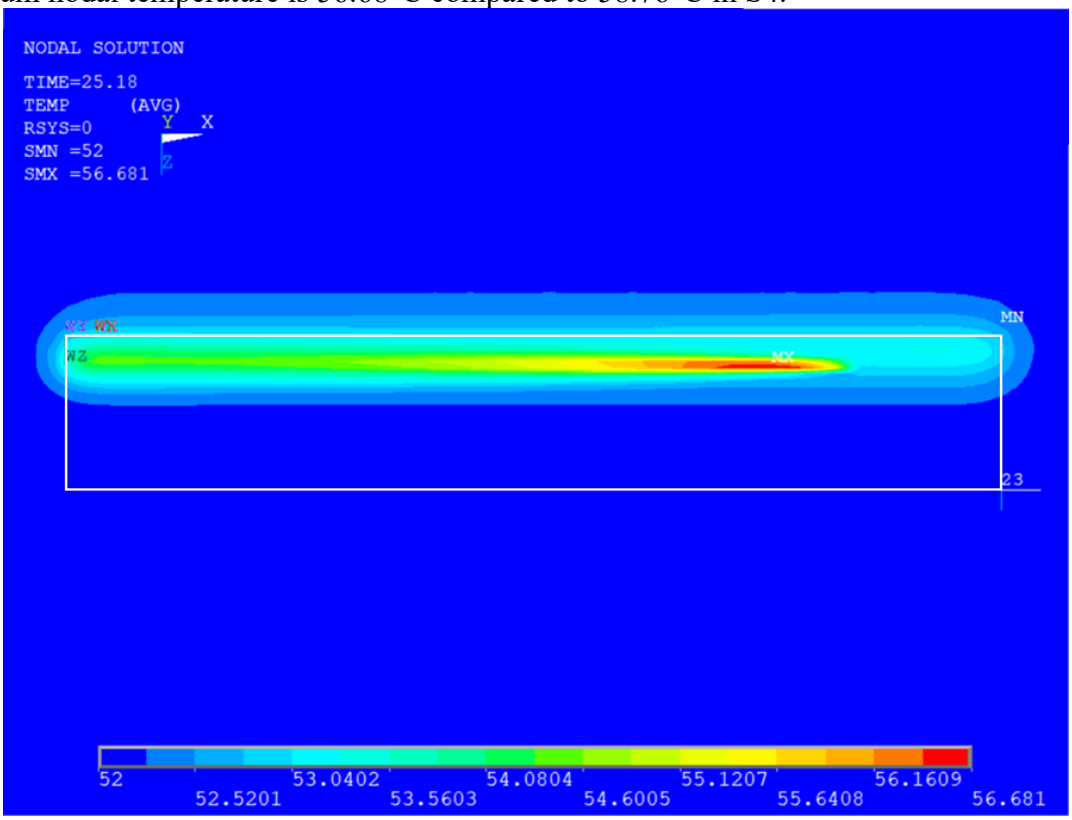

A)

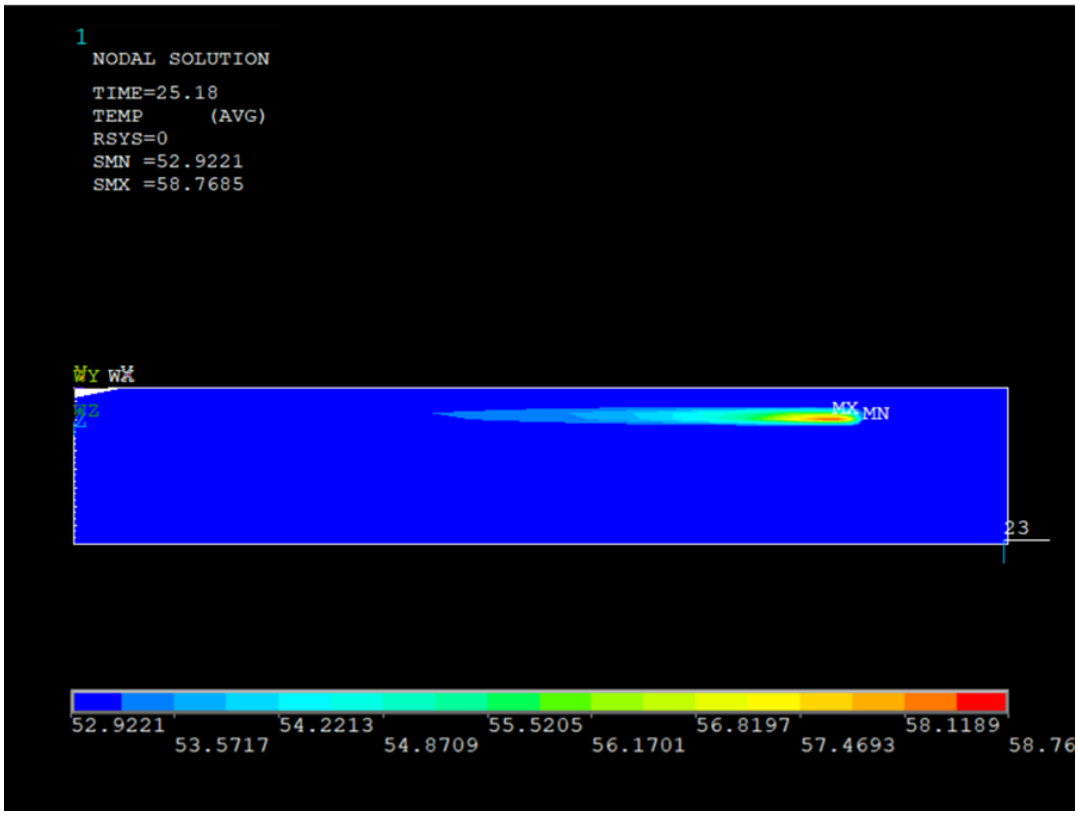

B)

Figure 4. Nodal contour plots, A) Nodal contour plot for time at 25.18 seconds for 100 mm x100 mm x 18 mm bed, B) Nodal contour plot for time at 25.18 seconds for 60 mm x10 mm x 0.2 mm bed

The next analysis focuses on the temperature change on the top face of the first layer elements and presented in Figure 5. These nodes demonstrate the influence of the attached nodes at y=0 mm and the penetration of thermal waves resulting from different applied boundary conditions. As observed, scenario S6 exhibits a slow cooling rate and does not reach the bed temperature of 52°C. This is mainly due to the dominance of the ambient temperature of 60°C, resulting from the higher heat transfer coefficient. Increasing the contact resistance to another extreme aids in improving the cooling rate, but the second observed peak is higher than in the other scenarios. This is a consequence of the higher activated temperature of the adjacent element nodes. However, it should be noted that the accuracy of temperature prediction in scenarios S6 and S7 is compromised due to the limitations of the contact conductance value.

Comparing scenarios S1, S2, S3, and S4, it is evident that the observed peaks in all cases are similar, but the cooling behavior of the elements differs for each scenario. As expected, the smallest bed size in S4 heats up and cools down rapidly due to its lower thermal mass, while faster cooldown rates in S1 and S2 are a result of the higher thermal mass. In contrast, scenarios S1 and S2, which have a higher thermal mass in the bed, experience faster cooldown due to the bed's ability to maintain a constant temperature throughout the process. This constant temperature aids in facilitating faster heat loss for the newly activated elements. On the other hand, scenario S3, with its optimal bed size, exhibits a slower heating rate while retaining heat for a longer duration. This prolonged heat retention allows the newly activated elements to remain at elevated temperatures

for an extended period. Lastly, scenario S5 closely approximates the temperature curves observed in the other scenarios, indicating its ability to provide accurate temperature predictions.

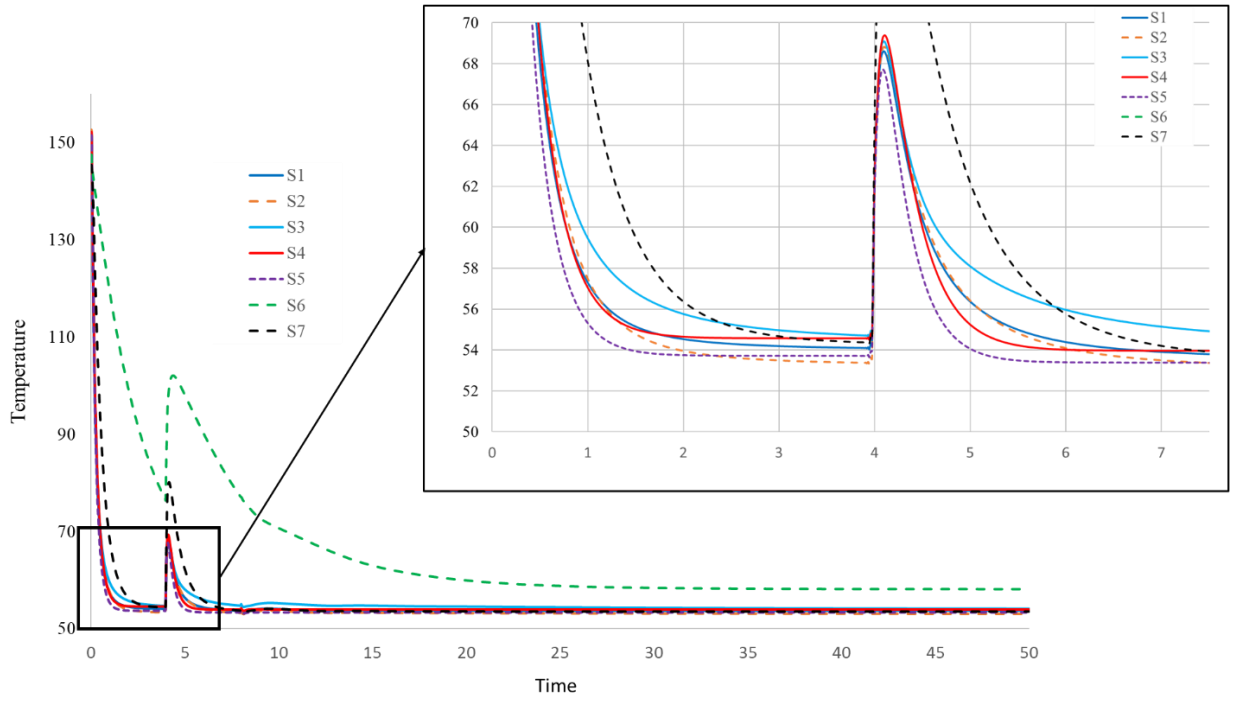

Figure 5. Variation of the temperature for the node at x=30 mm, z=5.2 mm, y=LH or 0.2 mm (on the bed)

In general, employing a constant bed temperature in simulations leads to decreased computational time due to the reduced Degrees of Freedom (DOF) required to solve for temperature variations. However, this approach still provides accurate temperature predictions. The primary challenge arises in accurately modeling the temperature of the attached nodes to the bed, which may result in errors of up to 7°C. Consequently, for thin parts, it is advisable to include print beds in the simulation process for more accurate results. This approach strikes a balance between computational efficiency and accuracy in temperature modeling.

Conclusion

The study investigated the impact of different boundary conditions applied to the print bed on both the nodes attached to it and the nodes of the first layer height elements. Sınce polymers have thermal conductivity in the order of $0.1\frac{W}{mK}$, thermal conductance value with the bed in the range of $1500\frac{W}{mK}$ gives the similar results and thus, thermal conduction with the print bed can be considered with less computational time. Otherwise, the thermal contact resistance must be calculated precisely by curve fitting to experimental results. Furthermore, three distinct conduction boundary conditions were tested, considering various dimensions of the print bed. The findings indicate that when reducing the size of the bed from its actual dimensions, the primary effect is

observed on the temperature of the attached nodes of the first layer, with a temperature difference of approximately 7°C. However, for nodes located on the top of the elements, the influence of the boundary conditions is less significant. In such cases, maintaining a constant bed temperature can be employed without significantly compromising the accuracy of the results.

References

1. Si H, Zhang Z, Huseynov O, et al (2023) Machine Learning-Based Investigation of the 3D Printer Cooling Effect on Print Quality in Fused Filament Fabrication: A Cybersecurity Perspective. Inventions 8:. https://doi.org/10.3390/inventions8010024
2. Fidan I, Imeri A, Gupta A, et al (2019) The trends and challenges of fiber reinforced additive manufacturing. 102:1801–1818
3. Alkunte S, Rajeshirke M, Fidan I, Hasanov S (2023) Performance evaluation of fatigue behavior in extrusion-based functionally graded materials. International Journal of Advanced Manufacturing Technology 128:863–875. https://doi.org/10.1007/S00170-023-11922-Z/METRICS
4. Rajeshirke M, Alkunte S, Huseynov O, Fidan I (2023) Fatigue analysis of additively manufactured short carbon fiber-reinforced PETG Components. International Journal of Advanced Manufacturing Technology 1–18. https://doi.org/10.1007/S00170-023-12107-4/METRICS
5. Fidan I, Huseynov O, Alshaikh Ali M, et al (2023) Recent Inventions in Additive Manufacturing: Holistic Review. Inventions 2023, Vol 8, Page 103 8:103. https://doi.org/10.3390/INVENTIONS8040103
6. Hasanov S, Alkunte S, Rajeshirke M, et al (2021) Review on Additive Manufacturing of Multi-Material Parts: Progress and Challenges. Journal of Manufacturing and Materials Processing 2022, Vol 6, Page 4 6:4. https://doi.org/10.3390/JMMP6010004
7. Ali MA, Fidan I, Tantawi K (2023) Investigation of the impact of power consumption, surface roughness, and part complexity in stereolithography and fused filament fabrication. International Journal of Advanced Manufacturing Technology 126:2665–2676. https://doi.org/10.1007/S00170-023-11279-3/METRICS
8. Huseynov O, Hasanov S, Fidan I (2023) Influence of the matrix material on the thermal properties of the short carbon fiber reinforced polymer composites manufactured by material extrusion. J Manuf Process 92:521–533. https://doi.org/10.1016/J.JMAPRO.2023.02.055
9. Das A, McIlroy C, Bortner MJ (2021) Advances in modeling transport phenomena in material-extrusion additive manufacturing: Coupling momentum, heat, and mass transfer. Progress in Additive Manufacturing 6:3–17. https://doi.org/10.1007/S40964-020-00137-3/METRICS
10. Costa SF, Duarte FM, Covas JA (2015) Thermal conditions affecting heat transfer in FDM/FFE: a contribution towards the numerical modelling of the process. Virtual Phys Prototyp 10:. https://doi.org/10.1080/17452759.2014.984042
11. Cattenone A, Morganti S, Alaimo G, Auricchio F (2019) Finite element analysis of additive manufacturing based on fused deposition modeling: Distortions prediction and comparison with experimental data. Journal of Manufacturing Science and Engineering, Transactions of the ASME 141:. https://doi.org/10.1115/1.4041626/367184

12. Prajapati H, Ravoori D, Jain A (2018) Measurement and modeling of filament temperature distribution in the standoff gap between nozzle and bed in polymer-based additive manufacturing. Addit Manuf 24:224–231. https://doi.org/10.1016/J.ADDMA.2018.09.030
13. Trofimov A, Le Pavic J, Pautard S, et al (2022) Experimentally validated modeling of the temperature distribution and the distortion during the Fused Filament Fabrication process. Addit Manuf 54:102693. https://doi.org/10.1016/J.ADDMA.2022.102693
14. Compton BG, Post BK, Duty CE, et al (2017) Thermal analysis of additive manufacturing of large-scale thermoplastic polymer composites. Addit Manuf 17:77–86. https://doi.org/10.1016/J.ADDMA.2017.07.006
15. Choo K, Friedrich B, Daugherty T, et al (2019) Heat retention modeling of large area additive manufacturing. Addit Manuf 28:325–332. https://doi.org/10.1016/J.ADDMA.2019.04.014
16. Friedrich BK, Choo K (2022) Thermal-Stress Characteristics of a Large Area Additive Manufacturing. https://doi.org/101080/0145763220222119919. https://doi.org/10.1080/01457632.2022.2119919
17. Ramos N, Mittermeier C, Kiendl J (2021) Experimental and numerical investigations on heat transfer in fused filament fabrication 3D-printed specimens. International Journal of Advanced Manufacturing Technology. https://doi.org/10.1007/s00170-021-07760-6
18. Nasirov A, Gupta A, Hasanov S, Fidan I (2020) Three-scale asymptotic homogenization of short fiber reinforced additively manufactured polymer composites. Compos B Eng 202:108269. https://doi.org/10.1016/j.compositesb.2020.108269
19. Farah S, Anderson DG, Langer R (2016) Physical and mechanical properties of PLA, and their functions in widespread applications — A comprehensive review. Adv Drug Deliv Rev 107:367–392. https://doi.org/10.1016/J.ADDR.2016.06.012
20. Çengel YA, Ghajar AJ (Afshin J Heat and mass transfer : fundamentals & applications. 1018